Taylor & Francis
Taylor & Francis Group

Journal of Maps

ISSN: (Print) (Online) Journal homepage: www.tandfonline.com/journals/tjom20

Geomorphology of craters located at Mercury's north pole

Silvia Bertoli, Alice Lucchetti, Maurizio Pajola, Elena Martellato, Matteo Massironi, Pamela Cambianica, Emanuele Simioni & Gabriele Cremonese

To cite this article: Silvia Bertoli, Alice Lucchetti, Maurizio Pajola, Elena Martellato, Matteo Massironi, Pamela Cambianica, Emanuele Simioni & Gabriele Cremonese (2024) Geomorphology of craters located at Mercury's north pole, Journal of Maps, 20:1, 2349788, DOI: 10.1080/17445647.2024.2349788

To link to this article: https://doi.org/10.1080/17445647.2024.2349788

JOURNAL OF MAPS
2024, VOL. 20, NO. 1, 2349788
https://doi.org/10.1080/17445647.2024.2349788

SCIENCE

OPEN ACCESS Check for updates

Geomorphology of craters located at Mercury's north pole

Silvia Bertoli[a,b], Alice Lucchetti[b], Maurizio Pajola[b], Elena Martellato[b], Matteo Massironi[c], Pamela Cambianica[b], Emanuele Simioni[b] and Gabriele Cremonese[b]

[a]Center of Studies and Activities for Space "G. Colombo" (CISAS), University of Padova, Padova, Italy; [b]INAF, Padova Astronomical Observatory, Padova, Italy; [c]Department of Geological Sciences, University of Padova, Padova, Italy

ABSTRACT

We present the first highly detailed morphological analysis of three craters located in Mercury's north pole, characterized by permanently shadowed regions (PSRs). This study, which began with an initial sample of 14 craters, highlighted three morphological classes, based on the craters' features: Complete complex morphology, Flat-floor morphology, and Immature complex morphology, presented here as maps of three representative craters, one for each class. As demonstrated by decades of studies, areas of PSRs within these craters could host water ice deposits, making them among the most interesting targets for future studies by the ESA/JAXA's BepiColombo mission. Our mapping work aims to give a cartographic context to subsequent chronological, thermal, and compositional analyses, as well as to provide a support to the acquisition strategy of the BepiColombo mission upon its arrival on Mercury in late 2025. The mapping highlights landforms which might be related to volcanic, gravitational, and maybe periglacial events.

ARTICLE HISTORY
Received 5 March 2024
Revised 24 April 2024
Accepted 25 April 2024

KEYWORDS
Cartography; Mercury; polar regions; craters; morphology

Key Science Highlights

- We present an in deep morphological analysis of craters located at north pole of Mercury using MDIS/WAC images.
- We identify three morphological classes based on the craters' features and morphologies.
- Trought photointerpretation analysis we provide the maps of three craters representative of the three classes, which can be used as a basis for future analysis.

1. Introduction

The planet Mercury, although visible to the naked eye and therefore known since antiquity, has long been an understudied planet due to the difficulties of observation. The first NASA's mission, Mariner 10, in 1974 has revealed the planet's surface for the first time. The spacecraft imaged about 40–45% of the planet's surface and several authors produced geological maps using these data (e.g. DeHon et al., 1981; Strom et al., 1990) dividing Mercury into 15 mapping quadrangles (Davies et al., 1978). Successively, the NASA's MESSENGER (MErcury Surface, Space ENvironment, GEochemistry, and Ranging, Solomon et al., 2007) spacecraft imaged at higher resolution the whole planet between 2011 and 2015 (Solomon et al., 2018). Based on this data, seven MESSENGER-based quadrangle maps at 1:3M scale have been published (e.g. Galluzzi et al., 2016; Giacomini et al., 2022). In addition, larger scale maps were produced for single features (e.g. Lucchetti et al., 2018; Pajola et al., 2021), allowing a more detailed investigation of their origin and evolution. However, detailed mapping can be more challenging, due to the uneven image resolution of some regions of interest and the lighting conditions which can greatly influence interpretation, especially on a large scale. Anyway, the resulting maps provide a good basis for identifying features of interest for other types of analysis such as dating, composition, and thermal modeling. In this work, we selected a sample of 14 craters located over 80°N in the north pole of Mercury, to study their morphology. These craters host permanently shadowed region (PSR) due to the planet's small obliquity (Margot et al., 2012), which are characterized by very low temperatures (less than 100 K, Paige et al., 2013). These conditions could have allowed the deposition and long-term survival of water ice, as suggested in the 90s after the discovery of radar bright material (hereafter called RBM) located within the PSRs by Earth-based radar observations (Harmon & Slade, 1992). This hypothesis was later corroborated through the comparisons with the signal from icy satellites and Mars's polar

CONTACT Silvia Bertoli silvia.bertoli@inaf.it Vicolo dell'Osservatorio 5, 35122, Padova (PD), Italy
Supplemental data for this article can be accessed online at https://doi.org/10.1080/17445647.2024.2349788

cap (Butler et al., 1993), hydrogen concentration on PSRs measured by the Neutron Spectrometer mounted on the MESSENGER mission (Harmon et al., 2011; Wilson et al., 2019), and thermal models (Paige et al., 2013). These craters are therefore very useful to investigate the presence of water ice (and/or volatiles in general) on a planet so close to the Sun. In fact, they have been included in the target list for the BepiColombo mission (Benkhoff et al., 2021). This list concerns targets of great scientific interest to which the attention and work of instruments will be devoted when BepiColombo arrives at Mercury at the end of 2025. The aim of this work is (1) to identify differences and similarities in the chosen crater sample, in terms of morphological appearance and landforms, and (2) to provide for the first time high-resolution geomorphological maps of craters located in Mercury's north pole. The objective is to create a cartographic basis for future studies (dating, thermal, and compositional), by the BepiColombo mission, in particular by the SIMBIO-SYS suite of remote sensing instruments (Cremonese et al., 2020).

2. Methods and techniques

2.1. Crater database

We selected the craters in the north pole area, above 80° N of latitude. We checked the available radar data on the MESSENGER Quick Map web-based mapping and analysis tool (https://mercury.quickmap.io), and selected craters using the following criteria: (1) availability of high-resolution MESSENGER Mercury Dual Imaging System (MDIS) images (Hawkins et al., 2007); (2) crater' diameters between 15 and 50 km to ensure a meaningful comparison between comparable craters and to unveil any crater complexity within a relatively broad size range; (3) low to moderate degradation degree to aid distinction of ejecta, floor, wall, and rim.

Following these criteria, a starting set of 14 craters was selected as shown in Figure 1. For more detailed information, see the Supplementary material, Table S1.

2.2. Dataset and projection

During its final year of operations, the MESSENGER mission acquired the highest-spatial-resolution views of Mercury's polar deposits (Chabot et al., 2016). For the photointerpretation, we selected the highest resolution wide-angle camera (WAC) images of the 14 craters (Table S2) by using the Planetary Image Locator Tool (PILOT, https://pilot.wr.usgs.gov/), an online data portal useful to search for images from the Planetary Data System (PDS) Cartography and Imaging Science Node. We excluded for our analysis the MDIS/narrow-angle camera (NAC) images provided by MESSENGER, because they have a non-uniform coverage and only a few craters are covered by this type of data. For each crater, we selected the image acquired with filter 7 (filename G, wavelength 748.7 nm) as a context image, some images acquired with filter 9 (Filename I, wavelength 996.2) to improve the coverage, plus a series of images acquired with filter 1 (filename B, wavelength 700 nm) for a more detailed view of the PSRs. In fact, even if they are in shadow, MESSENGER imaging system is enough sensitive to obtain images of the deposit surfaces with the very low levels of light scattered from surrounding illuminated topography They are taken with long exposures using the broadband star tracker clear filter (Chabot et al., 2014). The image details are in the Supplementary material (Table S2). The choice of these filters was influenced by the availability of data. By exploiting images with a resolution between 24 and 110 m/px, we were able to distinguish the surface features and to make an in-depth landscape analysis. As the craters are located above the 80°N, it is conventional to use a north stereographic projection (Davies et al., 1978). As a reference datum, we used a sphere with a radius of 2439.4 km (IAU 2015 report). We used the north polar Digital Elevation Model (DEM) derived from Mercury Laser Altimeter (MLA, Cavanaugh et al., 2017) to extract the topographic information of the craters (250 m/px of spatial resolution). We prefer to use the gridded data instead of individual MLA data tracks because the suitable tracks are not available for all the craters.

2.3. Morphological mapping

We performed the geomorphological mapping of the craters using a mapping scale based on USGS guidelines to achieve the final output scale of 1:250,000. The mapping approach follows the photointerpretation technique. We organized vector layers for digitization using QGIS 3.22. We divided the features into Landforms (divided by morphogenetic agent) and Units (divided according to their position within the crater). Our approach partly differs from the one adopted for mapping Mercury quadrangles (e.g. Galluzzi et al., 2016, 2019; Giacomini et al., 2022; Guzzetta et al., 2017; Mancinelli et al., 2016; Wright et al., 2019). In fact, the larger scale of this work allows the smaller landforms mapping (such as individual landslides) within the craters. Thus, the legend and its organization follow the logic of terrestrial geomorphological mapping and includes different colors depending on the morphogenetic agents. The colors and graphics of the landforms follow the geomorphological Earth legend of Campobasso et al. (2018). Red was used for gravitative landforms, which comprise linear elements such as the Crown, the undisplaced material still in place and adjacent to the highest parts of the main scarp, the Edge of the terrace and

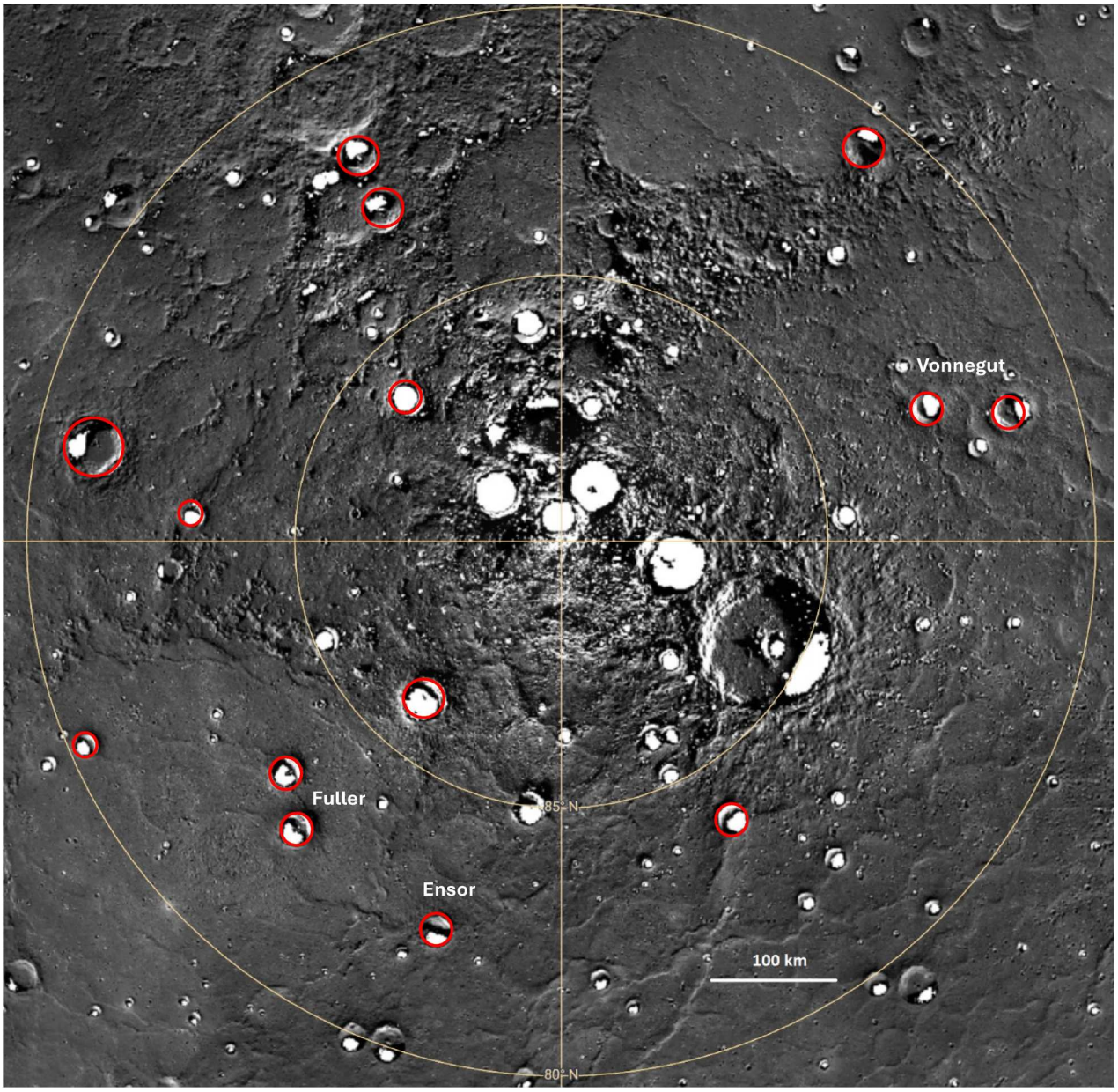

Figure 1. The red circles indicate the craters analyzed as the starting point of the research work and we labeled the three craters in which we focused in this study; the white patches represent the PSR. The north pole BDR basemap (166 m/px) is in stereographic projection centered at 90°N; 0°E (data of PSR taken from Harmon et al., 2011).

the Trench, and areal elements like the Landslide. Pink was chosen for the impact landforms, which commonly refers to 'Other landforms' on Earth, where impact morphologies are rare. We mapped all the craters, underlying or superimposed, as morphological elements which indicate an impact and the crater chains. We divided them between craters with diameter (D) > 20, which are the three main craters and craters with D < 20 km, which correspond to all the small impact in the images. For Fuller crater, black represents the 'Landform of uncertain origin'. For the radar data in raster format the 'Polygonise' tool in QGIS was used, in order to transform individual pixels of the raster into polygons. Then, to discriminate individual radar bright material (RBM) deposits, we merged the polygons belonging to the same deposit to form a unique polygon for each of them. In this way, the created vector layer could be easily overlaid on the maps to verify its relationship with respect to other units. They are mentioned in the legend as RBM'. We defined a 'dark material' (hereafter called DKM) unit, what Chabot et al. (2014) called the 'low reflectance material', which is associated with the RBM. The name 'low reflectance material' on Mercury normally refers to the oldest dark unit on the surface (Klima et al., 2018), hence we did not use this name in our map to avoid any misinterpretation.

3. Results

We first considered how the studied craters can be classified in terms of morphology. The impact

structures analyzed in this work have diameters between 17 and 47 km and are all complex craters. In fact, in the case of Mercury, the simple to complex transition diameter is about 12 km (Barnouin et al., 2012; Susorney et al., 2016). Complex craters would present a specific morphology, displaying flat floors, central peaks or peak rings, and terraced walls (e.g. Melosh, 1989; Susorney et al., 2016). However, our analysis highlighted a broad variation in terms of geomorphological complexity, which can be generalized into three different classes (here after named Class A, Class B, Class C) whose main characteristics are shown in Table S3. We decided to present the final output as maps of Fuller, Ensor and Vonnegut, which are craters representative of these three classes. They are presented in scale of 1:250,000 as printed version and as digital output (we refer to ZENODO repository, you can find the link in the Supplementary material).

In the following subsections, we describe the three classes and for each one, the representative crater and its features.

3.1. Class A – complete complex morphology

The first group of five craters presents a well-defined and sharp central peak (height > 500 m), a flat floor, and crater walls with evident terraces and trenches formed during gravitational collapse in the modification stage (class 'A' in Table S3). Central Peaks 500 m height are indicative of well-preserved and possibly younger craters.

3.1.1. Fuller

Fuller crater (Figure 2(A)), located at 82.6°N, 317.4°E, and with a diameter of 26.7 km, presents landforms related to gravitational, impact and uncertain processes.

It has a very well-developed central peak with steep slopes, clearly visible in the high-resolution MDIS image (Figure 2(B)) and in the topographic profile (check the white line in Figure 2(A) for the position, the profile is shown in Figure 2(G)). The northern part of its flat floor is occupied by a 110 km^2-wide landslide body (Figure 2(A–C)). The floor is covered by a few subsequent smaller craters, suggesting a low degradation stage for Fuller crater. It seems to be covered by DKM, which is spread from the base of the central peak up to the southern wall (Figure 2(B)) with well-defined contacts (Figure 2(D)). Furthermore, it presents peculiar linear features that recall fractures intersecting each other (Figure 2(E)), which we observe only in one other crater of this class. We classified these features as 'Landforms of Uncertain origin' because their morphogenesis cannot be unambiguously defined at the available resolution. Most of these structures seem to be aligned with four nearby outcropping rocks. These rocks (350 m long, following the main axis) have an asymmetrical shape, characterized by an elongated (and less sloping) shape in one direction and a shorter (and steeper) shape in the opposite direction. These shapes could be indicative of the direction of a possible flow process. We propose that permafrost and the related periglacial processes could be responsible of such features. On Earth, permafrost forms when ground is frozen for more than two years (Dobinski, 2011). We know that the craters with PSRs have a characteristic lag deposit on their floor, defined as dark carbon rich-material, representing the residue of sublimated ice (e.g. Paige et al., 2013; Syal et al., 2015). This layer could act as a permafrost active layer, which flows and produces cracks on the surface when assuming that the freeze cycle in penumbra areas is affected by heat transfer from the closeby permanently illuminated area (Filacchione et al., 2022). Regardless, we cannot exclude the possibility that fractures could be instead related to the cooling of impact melt material, which is a typical landform observed on Mercury (Xiao et al., 2014b).

The southern part of the crater floor is characterized by a hummocky, rough material, downslope from the central peak. This material is interesting because, due to its location, it could appear to be a landslide or something originating from the central peak. However, the texture is very rough and different from the other landslides we observe on the crater walls. Due to its shape, it could resemble a terrestrial rock glacier or a debris-covered glacier. The ejecta deposit is clearly asymmetrical, presenting in the western part smooth surface areas (Figure 2(F)), like melt pools. The Wall units comprise the smooth part of the wall, located close to the rim and the Terraced material unit. The Terraced material unit seems connected with the crater collapses and is indicative of Class A craters.

3.2. Class B – flat-floor morphology

The second group comprises three craters, having the characteristic flat floor of complex craters but lacking any CP in its floor or gravitational collapse along the crater walls (case 'B' in Table S3).

3.2.1. Vonnegut

Vonnegut (Figure 3(A)), located at 82.7°N, 110°E on the smooth plains, is a 26.2 km-diameter crater. It presents impact-related landforms and few gravitational processes. From Figure 3(B) and the topographic profile in Figure 3(E), it is clear the absence of CP within the flat floor and the presence of a smooth wall with only one main terrace located in the eastern part of the rim. Furthermore, in this portion, the rim appears smoother (see Figure 3(A)). The crater profile along a SE-NW trace (Figure 3(E)), highlights steep crater walls. DKM unit extends through the center of the floor up to the crater wall, in particular in the northern side (indicated by the white arrow in Figure

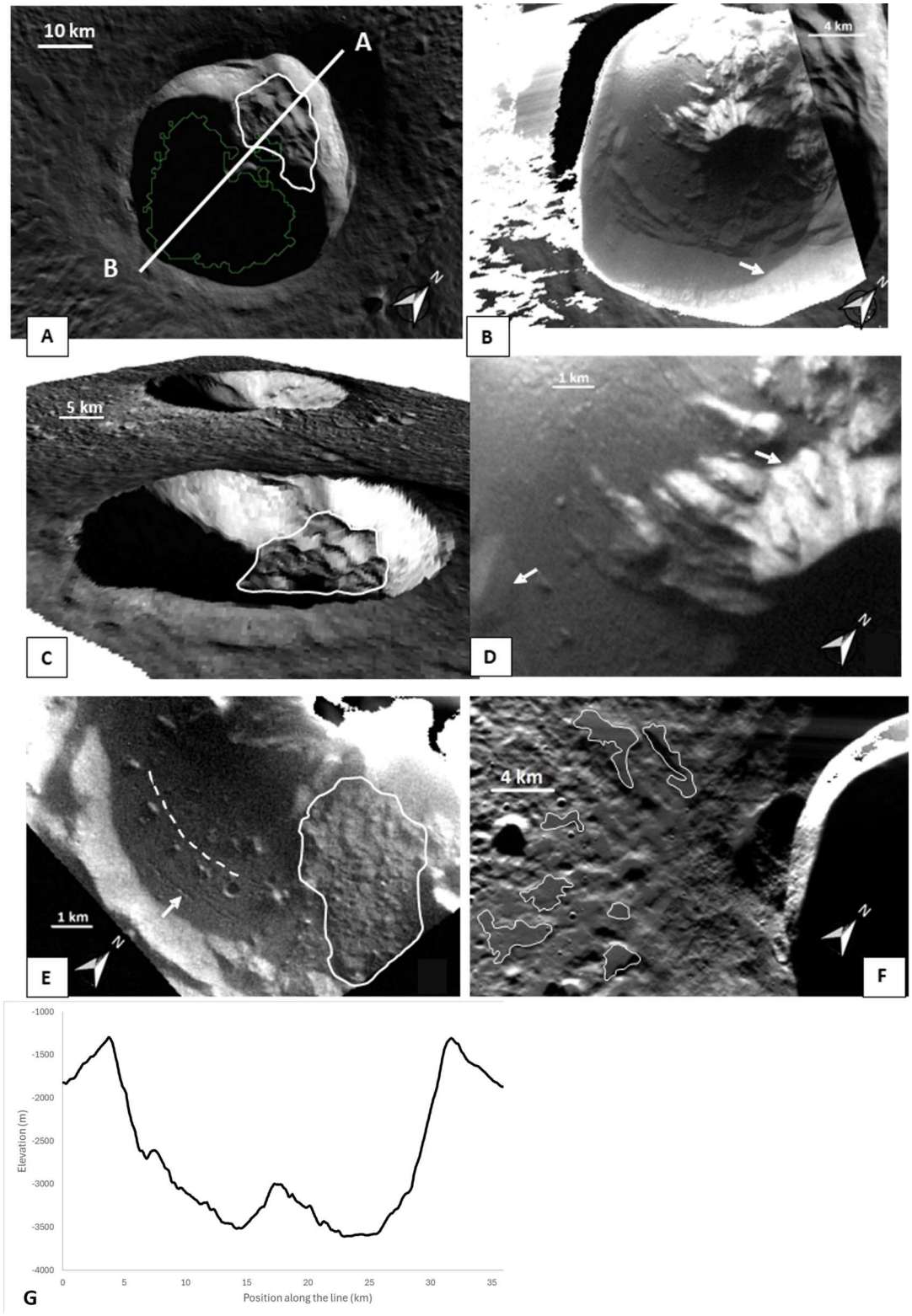

Figure 2. (A) Fuller crater overview: the white polygon indicated the landslide; the white line is the profile trace visible in Figure 2G and the green polygon indicated the PSRs. (B) An overview of the crater inner part, where the central peak and the flat floor are shown. The white arrow indicates the contact of the DKM and the surroundings. (C) A 3D model of the crater showing, outlined in white, a landslide body. (D) A high-resolution view of the central peak, with well-defined sharp walls. Note the contacts of dark material resting over the terraced material (left white arrows) and over the central peak's bottom (the right white arrow). (E) A high-resolution view of the floor. The white arrow indicates one of the fractures described in the main text. The dashed line points the direction of a possible 'flow'. In the right side of the image, a rough part of the floor (outlined with a white line) shows hummocky structures with few impacts. (F) Details of the proximal ejecta, where the white lines outline the melt pools. (G) Fuller's topographic profile (10x vertical exaggeration) shows the CP and the landslide body in the northern wall (left side on the panel).

3(B)). The ejecta blanket is barely distinct from the surrounding terrains.

Although no volcanic-like material has been unequivocally identified, a volcanic infilling might

have occurred in Vonnegut crater, where the possible channel of infilling could be located in the NW sector of the rim, which it seems more degraded. From buried and partially buried craters located in the Northern Smooth Plains (NSPs), several authors inferred that at least two episodes of volcanic resurfacing have occurred in this region (e.g. Denevi et al., 2013; Head et al., 2011). The estimated thickness of the NSP is 0.7–1.8 km, with a minimum volume of volcanic material of 4×10^6 to 107 km^3 (Ostrach et al., 2015). Therefore, a volcanic source external to the crater seems to be very likely. We cannot exclude also the erosion, which could have played an important role in crater modification. Indeed, it was shown that on Mercury crater degradation and topography evolution is twice faster than on the Moon. In particular, the speed rate of this process on Mercury is ~17 m^2/Myr over the last 3 Ga, about twice the value for the Moon (Fassett et al., 2017). In an atmosphereless

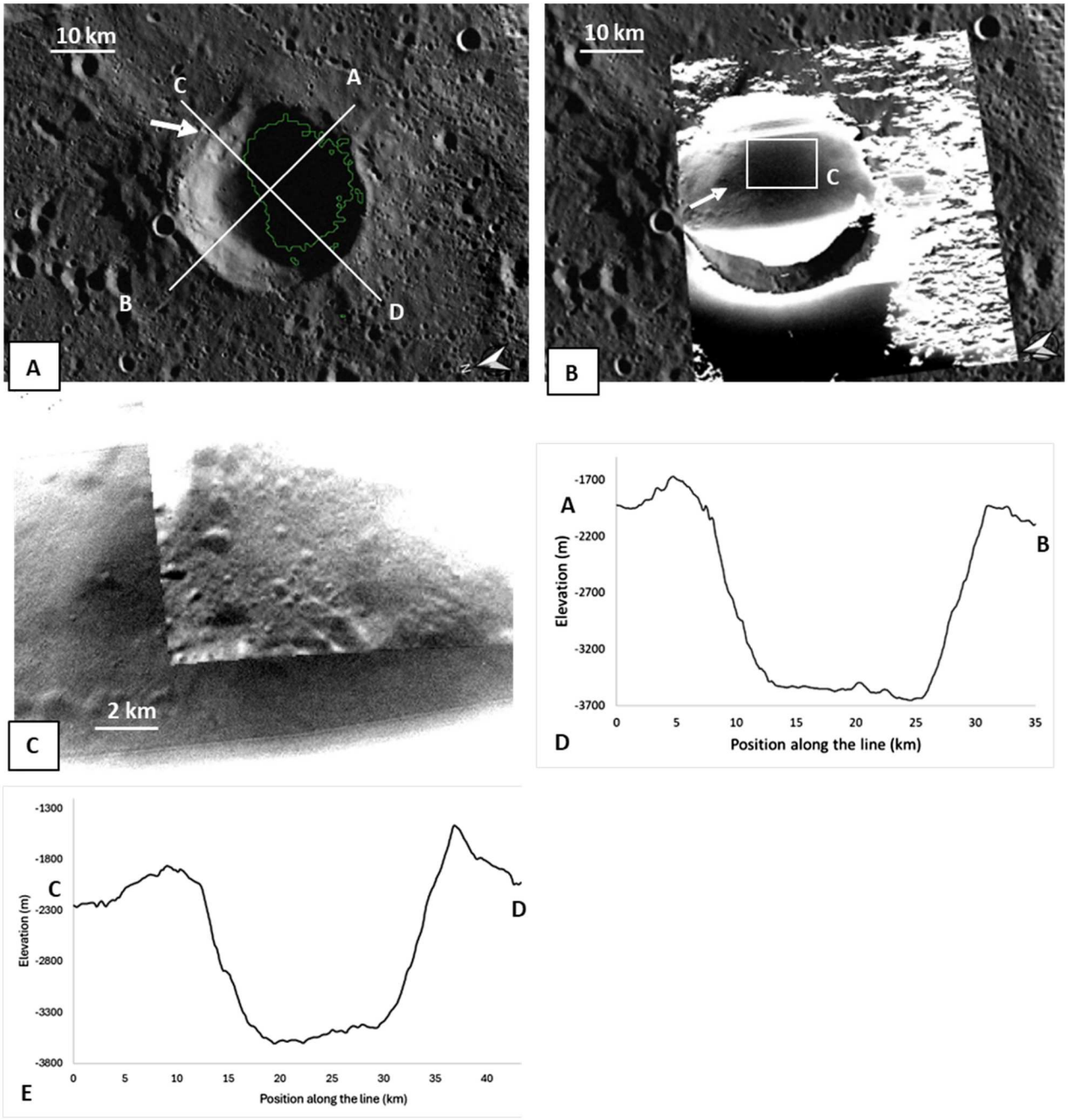

Figure 3. (A) Vonnegut crater characterized by an eroded, smooth edge and the left wall without clear gravitational structures but with small impacts. The white arrow indicates the part of the wall more degraded, visible also in the crater profile in E. The green polygon indicates the PSR and the white line indicated the position of the topographic profile of Figure 3E. (B) The stretched image shows the inner part of the crater, visible in detail in Figure 3C. (C) A detailed view of the shadowed part of the floor. The image shows many impact craters and the DKM (the contact indicates by the white arrow). (D) Topographic profile (10x vertical exaggeration) A-B shows very steep walls, lacking gravitational landforms, and a flat floor. (E) The second topographic profile which shows the altimetry difference of about 500 m between the northeastern and southwestern rim.

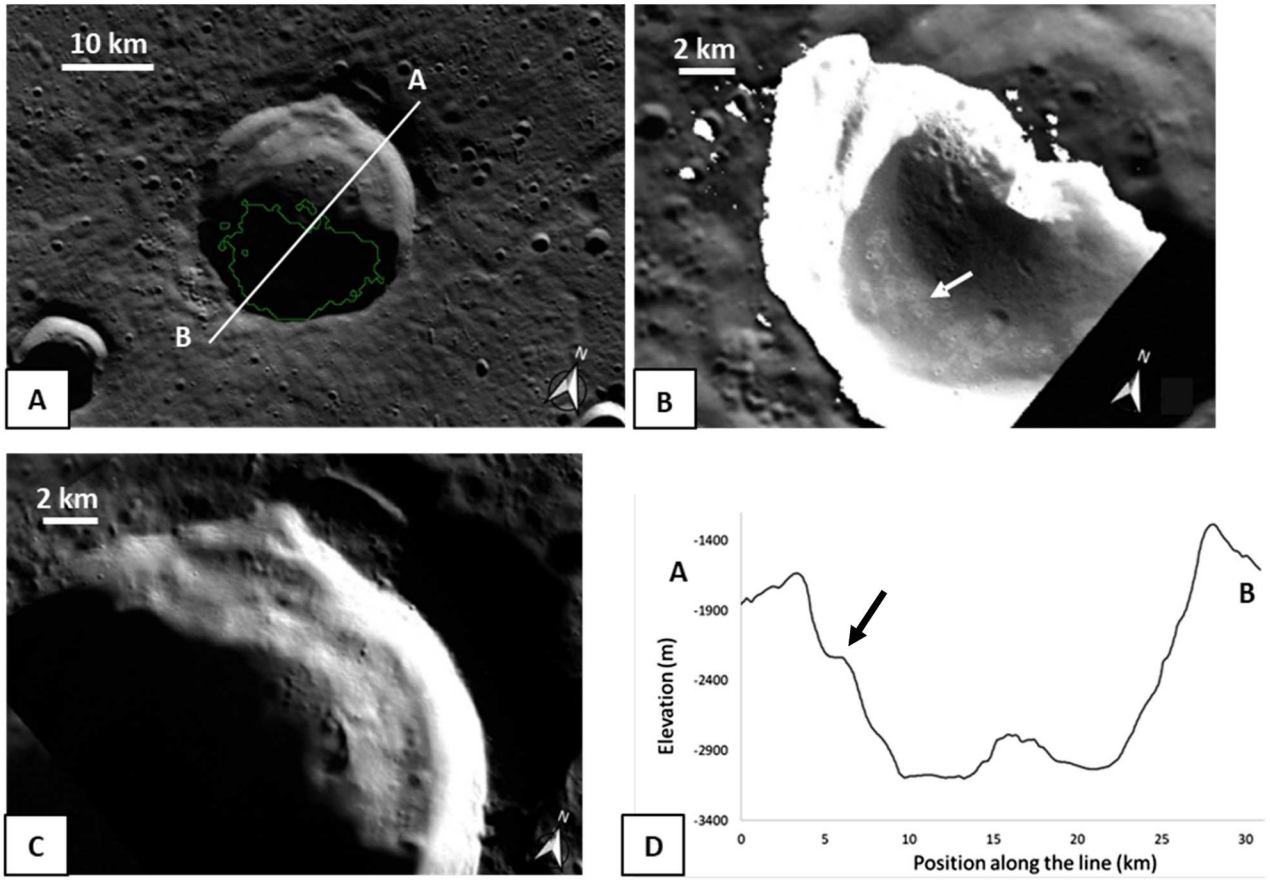

Figure 4. (A) An overview of Ensor crater. (B) The bright ejecta around the small impact crater in the wall of Ensor (white arrow). (C) A detailed view of Ensor wall. (D) Profile of the Ensor crater (10× vertical exaggeration). It shows 50 m of elevation difference between the shadowed part and the opposite illuminated part of the floor. The black arrow indicates the terraced wall.

planet the main agent of erosion is cratering itself, and its effect depends on the impact rate (Melosh, 1989).

3.3. Class C – immature complex

The third and last group includes six craters, which have attributes in between the other two groups (case 'C' in Table S3). They have terraces along their walls, flat floors, but only small CP (height < 500 m). The rim presents evident signs of erosion or partial resurfacing, suggesting that post-impact degradation might have modified the initial impact structure.

3.3.1. Ensor

Ensor crater (Figure 4(A)) is located at 82.3°N, 342.5°E, 24.5 km in diameter and presents few gravitational landforms. It presents a flat floor (Figure 4(B)), a 390-meter-high CP, and a terraced wall. The northern wall has a slight terrace and many small impacts (Figure 4(C)). Ensor presents bright ejecta associated to small impact craters, which is supposed to be exposed water ice (Deutsch et al., 2019). These overlay the crater's pole-facing wall (Figure 4(B)), which indeed returns a radar bright signal. Overall, the RBM occupies both the wall and part of the floor. The NW-SE cross-sectional topographic profile (Figure 4(D)) reveals that the floor fraction in PSR (marked as a thick black line) appears higher than the opposite side with respect to the CP, with a difference of approximately 50 m.

4. Summary and conclusion

We selected and analyzed 14 craters on Mercury, located at latitudes above 80°N. For each crater, we performed for the first time a high detailed morphological mapping, which allowed to distinguish them into three mains classes, based on their morphological features. These results are summarized in the maps of three craters, which are representative of the classes.

The first class includes craters with a completely developed complex morphology instead the second and third classes comprise craters without or with only a small CP, non-terraced wall, and with a more degraded morphology. Such an immature complex (Pike, 1988) morphology could be ascribed to post-impact modification processes, which would be able to obscure any CP. The main morphogenetic agents considered in this work for crater modification are gravity, volcanic activity, glacial/periglacial processes, and erosion. Alternatively, the immature complex morphology can develop during the impact process, as effect of the target and/or projectile properties, resulting in a transitional crater.

Those maps could be used as starting point for many analyses to understand better the occurrence and origin of the ice in the PSRs. As an example, the ejecta and others significant units within the crater could be very useful to have a better idea of the chronological order of the events by applying the crater counting method. Furthermore, the units and landforms can be better characterized by investigating both the illumination and thermal conditions affecting those areas. (e.g. investigating the possible presence of periglacial process). These maps will also be useful for adding other interesting targets to the list for SIMBIO-SYS, such as areas within Fuller and understand better the possible periglacial processes on Mercury. When BepiColombo will arrive on Mercury, the entire suite of SIMBIO-SYS instrument will be very helpful in better understanding the interiors of craters. SIMBIO-SYS/VIHI (Filacchione et al., 2020), in fact will offer a map of the ice composition, abundance, and grain size from visible and infrared observations and with SIMBIO-SYS/STC (Simioni et al., 2019) we will have the opportunity of performing accurate morphometric analyses of central peaks and landslides.

Software

QGIS 3.22 software was used to produce the Main Map.

Acknowledgements

This activity has been realized under the BepiColombo ASI-INAF contract no 2017- 47-H.0

Disclosure statement

No potential conflict of interest was reported by the author(s).

References

Barnouin, O. S., Zuber, M. T., Smith, D. E., Neumann, G. A., Herrick, R. R., Chappelow, J. E., Murchie, S. L., & Prockter, L. M. (2012). The morphology of craters on Mercury: Results from MESSENGER flybys. *Icarus*, *219* (1), 414–427. https://doi.org/10.1016/j.icarus.2012.02.029

Benkhoff, J., Murakami, G., Baumjohann, W., Besse, S., Bunce, E., Casale, M., Cremonese, G., Glassmeier, K.-H., Hayakawa, H., Heyner, D., Hiesinger, H., Huovelin, J., Hussmann, H., Iafolla, V., Iess, L., Kasaba, Y., Kobayashi, M., Milillo, A., Mitrofanov, I. G. … Zender, J. (2021). BepiColombo - Mission overview and science goals. *Space Science Reviews*, *217*(8), 90. https://doi.org/10.1007/s11214-021-00861-4

Butler, B. J., Muhleman, D. O., & Slade, M. A. (1993). Mercury: Full-disk radar images and the detection and stability of ice at the North Pole. *Journal of Geophysical Research: Planets*, *98*(E8), 15003–15023. https://doi.org/10.1029/93JE01581

Campobasso, C., Carton, A., Chelli, A., D'Orefice, M., Dramis, F., Graciotti, F., Guida, D., Pambianchi, G., Peduto, F., & Pellegrini, L. (2018). Aggiornamento ed integrazioni delle linee guida della carta geomorfologica d'Italia alla scala 1:50.000. *Progetto CARG Quaderni serie III*, *13*, 15–26.

Cavanaugh, J. F., Smith, J. C., Sun, X., Bartels, A. E., Ramos-Izquierdo, L., Krebs, D. J., McGarry, J. F., Trunzo, R., Novo-Gradac, A. M., Britt, J. L., Karsh, J., Katz, R. B., Lukemire, A. T., Szymkiewicz, R., Berry, D. L., Swinski, J. P., Neumann, G. A., Zuber, M. T., & Smith, D. E. (2017). The Mercury Laser Altimeter Instrument for MESSENGER mission. *Space Science Reviews*, *131*(1–4), 451–479. https://doi.org/10.1007/s11214-007-9273-4

Chabot, N. L., Ernst, C. M., Denevi, B. W., Nair, H., Deutsch, A. N., Blewett, D. T., Murchie, S. L., Neumann, G. A., Mazarico, E., Paige, D. A., Harmon, J. K., Head, J. W., & Solomon, S. C. (2014). Images of surface volatiles in Mercury's polar craters acquired by the MESSENGER spacecraft. *Geology*, *42*(12), 1051–1054. https://doi.org/10.1130/G35916.1

Chabot, N. L., Ernst, C. M., Paige, D. A., Nair, H., Denevi, B. W., Blewett, D. T., Murchie, S. L., Deutsch, A. N., Head, J. W., & Solomon, S. C. (2016). Imaging mercury's polar deposits during MESSENGER's low-altitude campaign. *Geophysical Research Letters*, *43*(18), 9461–9468. https://doi.org/10.1002/2016GL070403

Cremonese, G., Capaccioni, F., Capria, M. T., Doressoundiram, A., Palumbo, P., Vincendon, M., Massironi, M., Debei, S., Zusi, M., Altieri, F., Amoroso, M., Aroldi, G., Baroni, M., Barucci, A., Bellucci, G., Benkhoff, J., Besse, S., Bettanini, C., Blecka, M., … Turrini, D. (2020). SIMBIO-SYS: Scientific cameras and spectrometer for the BepiColombo mission. *Space Science Reviews*, *216*(5), 75. https://doi.org/10.1007/s11214-020-00704-8

Davies, M. E., Dornik, S. E., Gault, D. E., & Strom, R. G. (1978). *Atlas of Mercury*. NASA Special Publication.

DeHon, R. A., Scott, D. H., & Underwood, J. R. (1981). *Geologic map of the Kuiper quadrangle of Mercury*. USGS Misc. Investig. Ser. Map I–1233.

Denevi, B. W., Ernst, C. M., Meyer, H. M., Robinson, M. S., Murchie, S. L., Whitten, L. J., Head, J. H., Watters, T. R., Solomon, S. C., Ostrach, L. R., Chapman, C. R., Byrne, P. K., Klimczak, C., & Peplowski, P. N. (2013). The distribution and origin of smooth plains on Mercury. *Journal of Geophysical Research: Planets*, *118*(5), 891–907. https://doi.org/10.1002/jgre.20075

Deutsch, A. N., Head, J. W., & Neumann, G. A. (2019). Age constraints of Mercury's polar deposits suggest recent delivery of ice. *Earth and Planetary Science Letters*, *520*, 26–33. https://doi.org/10.1016/j.epsl.2019.05.027

Dobinski, W. (2011). Permafrost. *Earth-Science Reviews*, *108*(3-4), 158–169. https://doi.org/10.1016/j.earscirev.2011.06.007

Fassett, C. I., Crowley, M. C., Leight, C., Dyar, M. D., Minton, D. A., Hirabayashi, M., Thomson, B. J., & Watters, W. A. (2017). Evidence for rapid topographic evolution and crater degradation on Mercury from simple crater morphometry. *Geophysical Research Letters*, *44*(11), 5326–5335.

Filacchione, G., Frigeri, A., Raponi, A., Ciarniello, M., Capaccioni, F., De Sanctis, M. C., Carli, C., Galluzzi, V., Cremonese, G., Lucchetti, A., Re, C., & Massironi, M. (2020). Temporal evolution of the permanent shadowed regions at Mercury poles: Applications for spectral detection of ices by SIMBIOSYS-VIHI on BepiColombo mission. *Monthly Notices of the Royal Astronomical Society*, *498*(1), 1308–1318. https://doi.org/10.1093/mnras/staa2379

Filacchione, G., Raponi, A., Ciarniello, M., Capaccioni, F., Frigeri, A., Galiano, A., De Sanctis, M. C., Formisano, M., Galluzzi, V., & Cremonese, G. (2022). Detection of icy species in Mercury's PSRs: Spectral simulations for SIMBIO-SYS/VIHI on BEPI COLOMBO. *EPSC Abstracts*, *16*, EPSC2022-191. https://doi.org/10.5194/epsc2022-191

Galluzzi, V., Ferranti, L., Massironi, M., Giacomini, L., Guzzetta, L., & Palumbo, P. (2019). Structural analysis of the Victoria quadrangle fault systems on Mercury: Timing, geometries, kinematics, and relationship with the high-Mg region. *Journal of Geophysical Research: Planets*, *124*(10), 2543–2562. https://doi.org/10.1029/2019JE005953

Galluzzi, V., Guzzetta, L., Ferranti, F., Di Achille, G., Rothery, D. A., & Palumbo, P. (2016). Geology of the Victoria quadrangle (H02), Mercury. *Journal of Maps*, *12*(sup1), 227–238. https://doi.org/10.1080/17445647.2016.1193777

Giacomini, L., Galluzzi, V., Massironi, M., Ferranti, L., & Palumbo, P. (2022). Geology of the Kuiper quadrangle (H06), Mercury. *Journal of Maps*, *18*(2), 246–257. https://doi.org/10.1080/17445647.2022.2035268

Guzzetta, L., Galluzzi, V., Ferranti, L., & Palumbo, P. (2017). Geology of the Kuiper quadrangle (H03), Mercury. *Journal of Maps*, *13*(2), 227–238. https://doi.org/10.1080/17445647.2017.1290556

Harmon, J. K., & Slade, M. A. (1992). Radar mapping of Mercury: Full-disk images and polar anomalies. *Science*, *258*(5082), 640–643. https://doi.org/10.1126/science.258.5082.640

Harmon, J. K., Slade, M. A., & Rice, M. S. (2011). Radar imagery of Mercury's putative polar ice: 1999–2005 Arecibo results. *Icarus*, *211*(1), 37–50. https://doi.org/10.1016/j.icarus.2010.08.007

Hawkins, S. E., Boldt, J. D., Darlington, E. H., Espiritu, R., Gold, R. E., Gotwols, B., Grey, M. P., Hash, C. D., Hayes, J. R., Jaskulek, S. E., Kardian, C. J., Keller, M. R., Malaret, E. R., Murchie, S. L., Murphy, P. K., Peacock, K., Prockter, L. M., Reiter, R. A., Robinson, M. S., … Williams, B. D. (2007). The Mercury dual imaging system on MESSENGER spacecraft. *Space Science Reviews*, *131*(1-4), 247–338. https://doi.org/10.1007/s11214-007-9266-3

Head, J. W., Chapman, C. R., Strom, R. G., Fassett, C. I., Denevi, B. W., Blewett, D. T., Ernst, C. M., Watters, T. R., Solomon, S. C., Murchie, S. L., Prockter, L. M., Chabot, N. L., Gillis-Davis, J. J., Whitten, J. L., Goudge, T. A., Baker, M. H., Hurwitz, D. M., Ostrach, L. R., Xiao, Z., … Nittler, L. R. (2011). Flood volcanism in the northern high latitudes of Mercury revealed by MESSENGER. *Science*, *333*(6051), 1853–1856. https://doi.org/10.1126/science.1211997

Klima, R. L., Denevi, B. W., Ernst, C. M., Murchie, S. L., & Peplowski, P. N. (2018). Global distribution and spectral properties of low-reflectance material on Mercury. *Geophysical Research Letters*, *45*(7), 2945–2953. https://doi.org/10.1002/2018GL077544

Lucchetti, A., Pajola, M., Galluzzi, V., Giacomini, L., Carli, C., Cremonese, G., Marzo, G. A., Ferrari, S., Massironi, M., & Palumbo, P. (2018). Mercury hollow as remnants of original bedrock materials and devolatilization processes: A spectral clustering and geomorphological analysis. *Journal of Geophysical Research: Planets*, *123*(9), 2365–2379. https://doi.org/10.1029/2018JE005722

Mancinelli, P., Minelli, F., Pauselli, C., & Federico, C. (2016). Geology of the Raditladi quadrangle, Mercury (H04). *Journal of Maps*, *5647*, 1–13.

Margot, J.-L., Peale, S. J., Solomon, S. C., Hauck, S. A. I. I., Ghigo, F. D., Jurgens, R. F., Yseboodt, M., Giorgini, J. D., Padovan, S., & Campbell, D. B. (2012). Mercury's moment of inertia from spin and gravity data. *Journal of Geophysical Research: Planets*, *117*, E12.

Melosh, H. J. (1989). *Impact cratering. A geologic process. Oxford monographs on geology and geophysics series no. 11*. Oxford University Press. https://doi.org/10.1017/S0016756800007068

Ostrach, L. R., Robinson, M. S., Whitten, J. L., Fassett, C. I., Strom, R. G., Head, J. W., & Solomon, S. C. (2015). Extent, age, and resurfacing history of the northern smooth plains on Mercury from MESSENGER observations. *Icarus*, *250*, 602–622. https://doi.org/10.1016/j.icarus.2014.11.010

Paige, D. A., Siegler, M. A., Harmon, J. K., Neumann, G. A., Mazarico, E. M., Smith, D. E., Zuber, M. T., Harju, E., Delitsky, M. L., & Solomon, S. C. (2013). Thermal stability of volatiles in the north polar region of Mercury. *Science*, *339*(6117), 300–303. https://doi.org/10.1126/science.1231106

Pajola, M., Lucchetti, A., Semenzato, A., Poggiali, G., Munaretto, G., Galluzzi, V., Marzo, G. A., Cremonese, G., Brucato, J. R., Palumbo, P., & Massironi, M. (2021). Lermontov crater on Mercury: Geology, morphology and spectral properties of the coexisting hollows and pyroclastic deposits. *Planetary and Space Science*, *195*, 105136. https://doi.org/10.1016/j.pss.2020.105136

Pike, R. J. (1988). Geomorphology of impact craters on Mercury. *Mercury*, 165–273.

Simioni, E., Da Deppo, V., Re, C., Slemer, A., Capria, M. T., Ficai Veltroni, I., Borrelli, D., Dami, M., Tommasi, L., Mugnuolo, R., Amoroso, M., Longo, F., & Cremonese, G. (2019). SIMBIO-SYS/STC stereo camera calibration: Geometrical distortion. *Review of Scientific Instruments*, *90*(4), 043106. https://doi.org/10.1063/1.5085710

Solomon, S. C., McNutt, R. L., Gold, R. E., & Domingue, D. L. (2007). MESSENGER mission overview. *Space Science Reviews*, *131*(1-4), 3–39. https://doi.org/10.1007/s11214-007-9247-6

Solomon, S. C., Nittler, L. R., & Anderson, B. J. (2018). *Mercury: The view after MESSENGER*. Cambridge University Press.

Strom, R. G., Malin, M. C., & Leake, M. A. (1990). *Geologic map of the Bach region of Mercury*. USGS Misc. Investig. Ser. Map I–2015.

Susorney, H. C. M., Barnouin, O. S., Ernst, C. M., & Johnson, C. L. (2016). Morphometry of impact craters on Mercury from MESSENGER altimetry and imaging. *Icarus*, *271*, 180–193. https://doi.org/10.1016/j.icarus.2016.01.022

Syal, M. B., Schultz, P. H., & Riner, M. A. (2015). Darkening of Mercury's surface by cometary carbon. *Nature Geoscience*, *8*(5), 352. https://doi.org/10.1038/ngeo2397

Wilson, J. T., Lawrence, D. J., Peplowski, P. N., & Feldman, W. C. (2019). MESSENGER gamma ray spectrometer and epithermal neutron hydrogen data reveal compositional differences between Mercury's hot and cold poles. *Journal of Geophysical Research: Planets*, *124*(3), 721–733. https://doi.org/10.1029/2018JE005871

Wright, J., Rothery, D. A., Balme, M. R., & Conway, S. J. (2019). Geology of Hokusai quadrangle (H05), Mercury. *Journal of Maps*, *12*(2), 509–520. https://doi.org/10.1080/17445647.2019.1625821

Xiao, Z., Zeng, Z., Li, Z., Blair, D. M., & Xiao, L. (2014b). Cooling fractures in impact melt deposits on the Moon and Mercury: Implications for cooling solely by thermal radiation. *Journal of Geophysical Research: Planets*, *119*(7), 1496–1515. https://doi.org/10.1002/2013JE004560